Contemporary Engineering Sciences, Vol. 9, 2016, no. 15, 713 - 725
HIKARI Ltd, www.m-hikari.com
http://dx.doi.org/10.12988/ces.2016.6434

L-Band SiGe HBT Dual-Band Differential Amplifiers Having Frequency-Tunable Bandpass or Bandstop Responses Using Novel Varactor-Loaded Dual-Band Resonators

Yasushi Itoh

Shonan Institute of Technology
1-1-25 Tsujido-Nishikaigan
Fujisawa, Kanagawa, 251-8511 Japan

Hiroaki Takagi

Shonan Institute of Technology
1-1-25 Tsujido-Nishikaigan
Fujisawa, Kanagawa, 251-8511 Japan

Abstract

L-band SiGe HBT dual-band differential amplifiers with frequency-tunable bandpass or bandstop responses have been developed for the next generation adaptive and/or reconfigurable wireless radios. A novel varactor-loaded dual-band resonator comprised of series and parallel LC circuits is employed in the load circuit of differential amplifiers for realizing dual-bandstop responses as well as the series feedback circuit for dual-bandpass responses. The dual-bandstop amplifier has presented a lower-bandstop frequency of 0.47 to 0.62 GHz with an upper-bandstop frequency of 1.17 to 1.18 GHz. Meanwhile, an upper–bandstop frequency can be varied from 0.6 to 1.1 GHz for a lower-bandstop frequency of 0.37 to 0.4 GHz. The maximal band-rejection was 17.7 dB. In addition, the dual-bandpass amplifier has achieved a lower-bandpass frequency of 0.37 to 0.5 GHz with an upper-bandpass frequency of 0.61 to 0.63 GHz. Meanwhile, an upper-

bandpass frequency can be varied from 0.61 to 1.11 GHz for a lower-bandpass frequency of around 0.36 GHz. The maximal gain was 9.6 dB. The varactor-loaded dual-band resonator presented in this paper is expected to be one candidate for realizing the multi-band amplifier utilized in the reconfigurable wireless transceivers.

Keywords: microwaves, multi-band, amplifier, LC resonator, SiGe HBT

1 Introduction

Recent evolutions of wireless communication system are going forward the 4G advanced LTE and 5G systems including the adaptive and/or reconfigurable multi-standard transceivers as well as higher speed and higher frequencies [1], [2]. The frequency spectrum becomes also wider from the traditional L/S-band up to millimeter-wave frequencies to meet a wide range of date rates over several frequency bands of wireless radios [3]. As the active radios are collocated in both frequency and space, the interference and image rejection becomes a crucial issue [4]. In the multi-band and multi-mode receiving operations, the image signals actually drop into the current frequency band which necessarily leads to time-frequency collisions and interferences. In order to meet these requirements, various types of multi-band amplifiers with bandpass or bandstop responses have been researched and developed. Most of the multi-band amplifiers with bandpass responses have focused on the concurrent amplification [5], including wideband matching [6], dual-band matching with a fixed frequency [7] and single-band matching with a tunable frequency [8]. On the other hand, various types of multi-band amplifiers with bandstop responses have been also reported, including active interference canceller [4], image rejection LNA [9], [10] and frequency-agile absorptive bandstop filter [11]. In order to enhance these performances, the authors have presented the dual-bandpass or dual-bandstop differential amplifiers having frequency-tunable capabilities with the use of the varactor-loaded stacked LC resonators [12], [13], [14]. These varactor-loaded stacked LC resonator can actually accomplish an independent frequency tuning but a frequency separation between dual-band frequencies was limited by the element value and thus frequency coverage becomes narrow. To address this problem, the varactor-loaded dual-band resonator comprised of series and parallel LC circuits was devised for the low-noise differential amplifier with bandpass or bandstop responses [15]. Since this resonator utilizes an open circuited condition in both the load and feedback circuits, the circuit stability becomes a serious problem. To address this issue, a novel varactor-loaded dual-band resonator is presented in this paper. It combines a dual-band LC resonator with a resistor for biasing and high stability and thus can provide dual-bandstop or dual-bandpass responses with high stability.

2 Dual-Band Resonator Using LC Circuits

A schematic diagram of the differential amplifier with the load circuit Z_L and the series feedback circuit Z_S is shown in Fig. 1. Since Z_S is connected between transistor pairs, two current sources are used. The balanced voltage gain G can be approximated as the following equation:

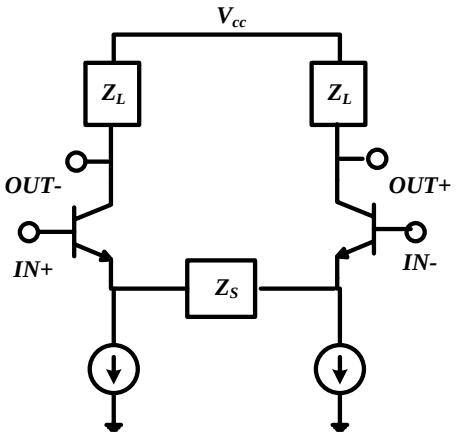

Fig.1 Schematic diagram of the differential amplifier with the load circuit Z_L and the series feedback circuit Z_S

$$G = \left| \frac{2Z_L}{Z_S} \right| \tag{1}$$

The maximal gain is obtained for an open-circuited Z_L or a short-circuited Z_S. In a similar way, the minimal gain is obtained for a short-circuited Z_L or an open-circuited Z_S. For example, LC resonators can make both open-circuited and short-circuited conditions and thus bandpass or bandstop responses can be realized at multiple bands when applied to Z_L or Z_S. Now it is assumed that the dual-band resonators using LC circuits are employed in the load circuit Z_L. Schematic diagrams of the dual-band resonators using LC circuits, frequency responses and resonant frequencies are summarized in Table 1. Type A combines dual parallel LC circuits in a stacked configuration. Since parallel LC circuits become open at resonant frequencies, the resonator shows dual bandpass and single bandstop responses. The resonant frequencies f_1 and f_2 can be varied independently with the use of the variable capacitances C_1 and C_2. On the other hand, type B combines dual series LC circuits in parallel. Since series LC circuits become short at resonant frequencies, the resonator shows dual bandstop and single bandpass responses. The resonant frequencies f_1 and f_2 can be also varied independently. Types C and D combines parallel and series LC resonators. As compared with Types A and B, the resonant frequencies f_1 and f_2 cannot be varied

independently. However, the frequency separation becomes larger [15]. The difference between Types C and D is in that series and parallel LC resonators are combined in parallel for Type C or in series for Type D. Type C provides dual bandpass and single bandstop responses but type D produces dual bandstop and single bandpass responses. The resonant frequencies f_1 and f_2 are the same but f_3 is different. Since each circuit element has a resistive value in actual cases, the circuit loss becomes larger for Type D because of the series connection of circuit elements. Table 1 shows the case in that the dual-band resonators are employed in the load circuit Z_L of the differential amplifier. In an application of the series feedback circuit Z_S, the frequency responses become just the opposite, as clearly shown in Equation 1. In this paper, the design, fabrication and performance of the dual-bandpass or dual-bandstop differential amplifier with the dual-band resonator of Type D are described.

Table 1 Schematic diagrams of the dual-band resonators using LC circuits, frequency responses and resonant frequencies

	Type A	***Type B***	***Type C***	***Type D***
Schematic Diagram	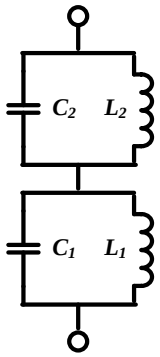	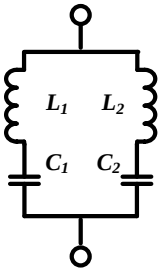	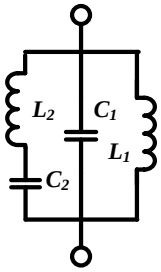	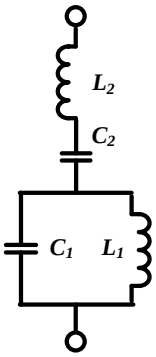
Response	***Dual-Bandpass*** 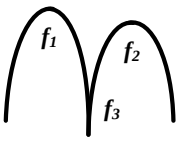	***Dual-Bandstop*** 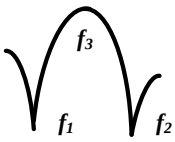	***Dual-Bandpass*** 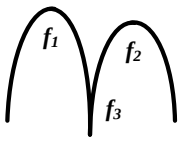	***Dual-Bandstop*** 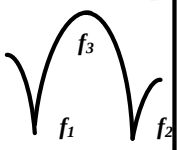
Resonant Frequencies	$f_1 = \frac{1}{2\pi\sqrt{L_2C_2}}$ $f_2 = \frac{1}{2\pi\sqrt{L_1C_1}}$ $f_3 = \frac{1}{2\pi}\sqrt{\frac{1/L_1+1/L_2}{C_1+C_2}}$	$f_1 = \frac{1}{2\pi\sqrt{L_2C_2}}$ $f_2 = \frac{1}{2\pi\sqrt{L_1C_1}}$ $f_3 = \frac{1}{2\pi}\sqrt{\frac{1/C_1+1/C_2}{L_1+L_2}}$	$f_1 = \frac{1}{2\pi}\sqrt{\frac{b-\sqrt{b^2-4a}}{2a}}$ $f_2 = \frac{1}{2\pi}\sqrt{\frac{b+\sqrt{b^2-4a}}{2a}}$ $f_3 = \frac{1}{2\pi\sqrt{L_2C_2}}$	$f_1 = \frac{1}{2\pi}\sqrt{\frac{b-\sqrt{b^2-4a}}{2a}}$ $f_2 = \frac{1}{2\pi}\sqrt{\frac{b+\sqrt{b^2-4a}}{2a}}$ $f_3 = \frac{1}{2\pi\sqrt{L_1C_1}}$
Ref.	[12], [13], [14]	[12], [13], [14]	[15]	This work

3 Dual-Bandstop Differential Amplifier

A schematic diagram of the L-band SiGe HBT dual-band differential amplifier having frequency-tunable bandstop responses is displayed in Fig. 2. The varactor-loaded dual-band resonator of Type D in Table 1 is employed in the output circuit Z_L to achieve dual-bandstop responses. L_1 and C_1 consists of a parallel LC resonator as well as L_2 and C_2 consists of a series LC resonator. C_1 and C_2 are a variable capacitance, as shown in Fig. 2. R_L is connected is parallel with the dual-band resonator for biasing and high stability. The value of R_L has to be carefully chosen for biasing and high stability. In consideration with the output matching, 56 ohms was finally chosen. A cascode connection of HBTs is used to achieve high gain as well as variable gain. V_{CC} and V_{B2} are a supply voltage and a control voltage of the 2nd base bias, respectively. The circuit element values are listed in Table 2.

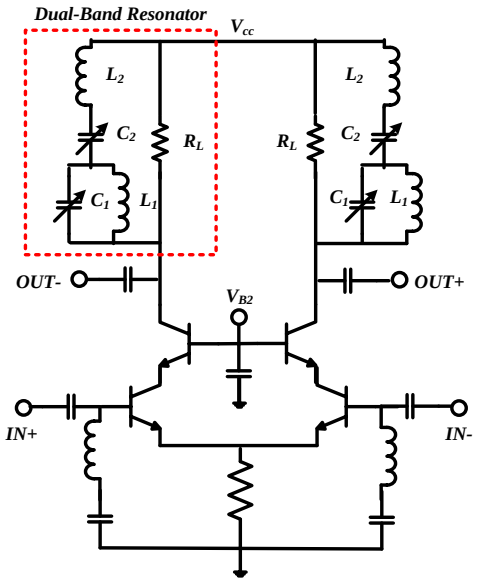

Fig.2 Schematic diagram of the L-band SiGe HBT dual-band differential amplifier having frequency-tunable bandstop responses

Table 2 Circuit element values

	Bandpass	Bandstop
Element	Value	Value
L_1 [nH]	2	4.7
C_1 [pF]	6 to 15	6 to 15
L_2 [nH]	2	5.6
C_2 [pF]	6 to 15	6 to 15

The resonant frequencies of f_1, f_2 and f_3 are calculated by using the equations of Type D listed in Table 1 as well as the circuit element values of Table 2. The calculation was done first for a variable C_1 and a fixed C_2. The calculated results are shown in Fig. 3. As clearly shown, f_1, f_2 and f_3 are varied with C_1. Moreover, the bandpass frequency f_3 is necessarily sandwiched between f_1 and f_2. Then the calculation was done for a variable C_2 and a fixed C_1. The calculated results are shown in Fig. 4. Contrary to Fig. 3, f_3 keeps constant. The bandpass frequency f_3 is also sandwiched by f_1 and f_2.

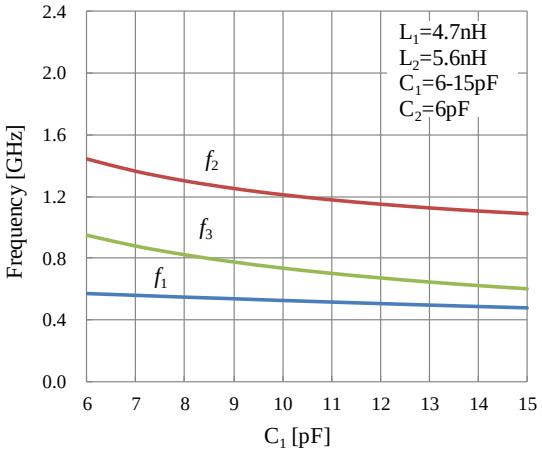

Fig.3 Calculated f_1, f_2 and f_3 for a variable C_1 and a fixed C_2

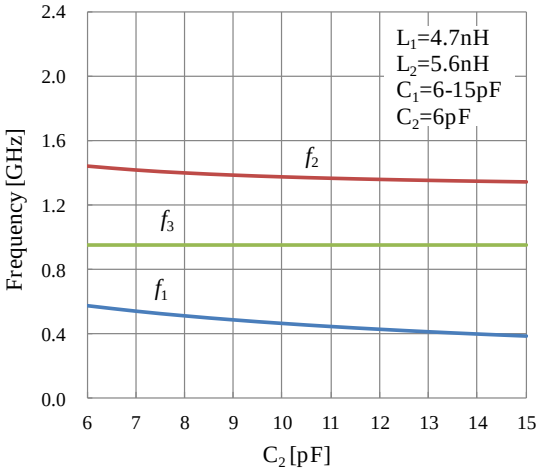

Fig.4 Calculated f_1, f_2 and f_3 for a variable C_2 and a fixed C_1

A photograph of the L-band SiGe HBT dual-band differential amplifier having frequency-tunable bandstop responses is displayed in Fig. 5. The amplifier was fabricated on the FR-4 substrate with a dielectric constant of 4.5. 1005-type chip

resistors, capacitors, and inductors are mounted on the substrate by soldering. A surface mount type of the 0.35 μm SiGe HBT with an f_t of around 25 GHz (Toshiba MT4S102T) and the Si varactor diode with a capacitance ratio of 2.5:1 (Toshiba 1SV279) are employed. The circuit size is 14 x 16 x 1.2 mm^3.

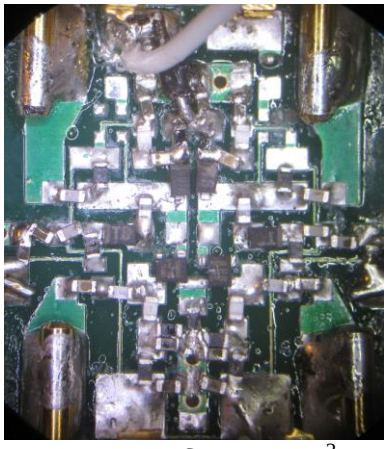

14 x 16 x 1.2 mm^3

Fig.5 Photograph of the L-band SiGe HBT dual-band differential amplifier having frequency-tunable bandstop responses

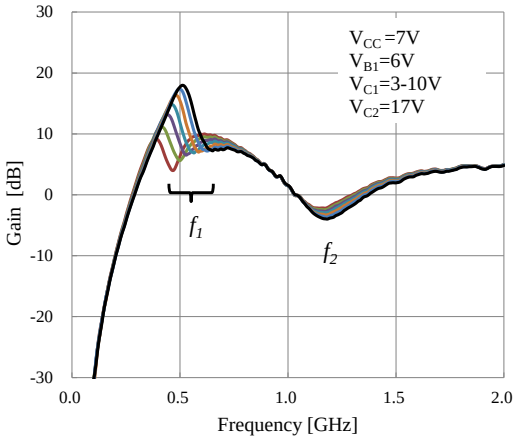

Fig.6 Measured gains of the L-band SiGe HBT dual-band differential amplifier having frequency-tunable bandstop responses for a variable C_1 and a fixed C_2

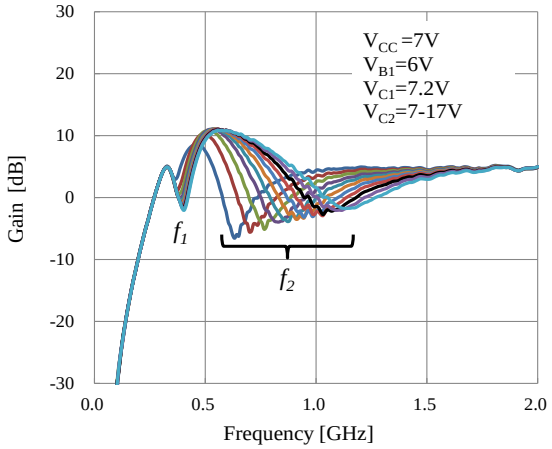

Fig.7 Measured gains of the L-band SiGe HBT dual-band differential amplifier having frequency-tunable bandstop responses for a variable C_2 and a fixed C_1

Measured gains of the L-band SiGe HBT dual-band differential amplifier having frequency-tunable bandstop responses are shown in Fig. 6 for a variable C_1 and a fixed C_2 as well as in Fig. 7 for a variable C_2 and a fixed C_1. In Fig. 6, the lower-bandstop frequency was varied from 0.47 to 0.62 GHz with an upper-bandstop frequency of 1.17 to 1.18 GHz. On the other hand, the upper-bandstop frequency can be varied from 0.6 to 1.1 GHz for a lower-bandstop frequency of 0.37 to 0.4 GHz in Fig. 7. The maximal band-rejection was 17.7 dB. The bias conditions for V_{CC}, V_{B2}, V_{C1} and V_{C2} are also shown in Figs. 6 and 7. A collector current was around 8mA.

4 Dual-Bandpass Differential Amplifier

A schematic diagram of the L-band SiGe HBT dual-band differential amplifier having frequency-tunable bandpass responses is demonstrated in Fig. 8. The varactor-loaded dual-band resonator of Type D in Table 1 is employed in the series feedback circuit Z_S to achieve dual-bandpass responses. L_1 and C_1 consists of a parallel LC resonator as well as L_2 and C_2 consists of a series LC resonator. C_1 and C_2 are a variable capacitance. R_L is connected is parallel with the dual-band resonator for high stability. The value of R_L has to be carefully chosen because there exists a tradeoff between stability and frequency-tuning capability. Therefore the value of R_L was finally chosen as 100 ohms for high stability. A cascode connection of HBTs is also used to achieve high gain as well as variable gain. The circuit element values listed in Table 2 are used.

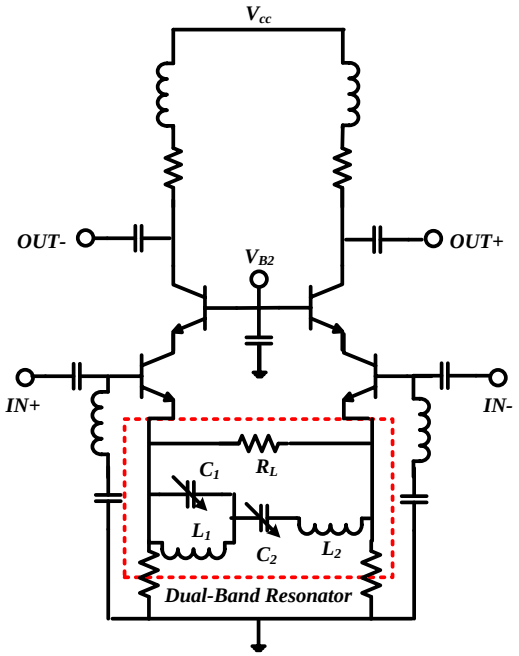

Fig.8 Schematic diagram of the L-band SiGe HBT dual-band differential amplifier having frequency-tunable bandpass responses

The resonant frequencies of f_1, f_2 and f_3 are calculated again because the circuit element values are different from the dual-bandstop amplifier. The calculation was done first for a variable C_1 and a fixed C_2. Then the calculation was done for a variable C_2 and a fixed C_1. The calculated results are shown in Fig. 9 for a variable C_1 and a fixed C_2 as well as Fig. 10 for a variable C_2 and a fixed C_1. As compared with Figs. 3 and 4, the calculated performances are similar.

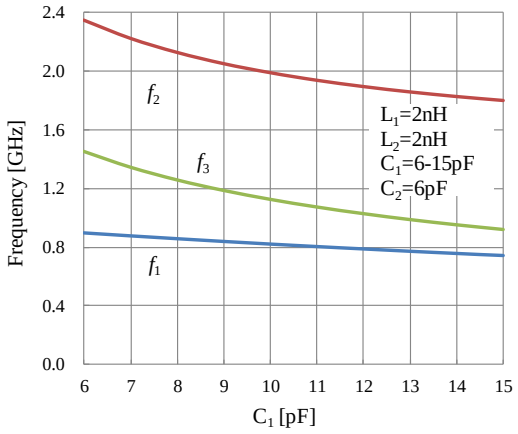

Fig.9 Calculated f_1, f_2 and f_3 for a variable C_1 and a fixed C_2

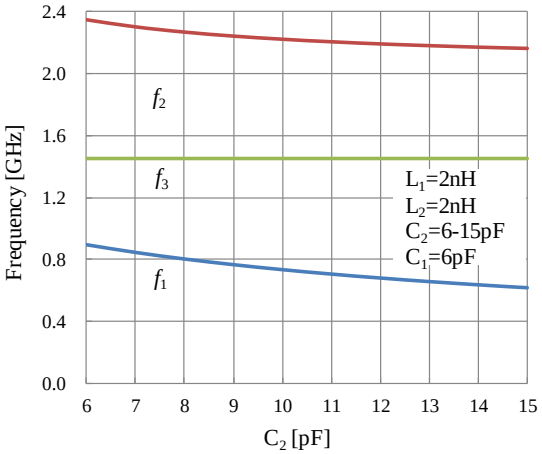

Fig.10 Calculated f_1, f_2 and f_3 for a variable C_2 and a fixed C_1

A photograph of the L-band SiGe HBT dual-band differential amplifier having frequency-tunable bandpass responses is shown in Fig. 11. The amplifier was fabricated on the FR-4 substrate with a dielectric constant of 4.5. 1005-type chip resistors, capacitors, and inductors are mounted on the substrate by soldering. A surface mount type of the 0.35 μm SiGe HBT with an f_t of around 25 GHz (Toshiba MT4S102T) and the Si varactor diode with a capacitance ratio of 2.5:1 (Toshiba 1SV279) are employed. The circuit size is 14 x 16 x 1.2 mm^3.

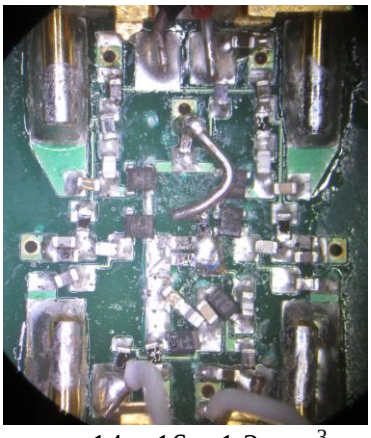

14 x 16 x 1.2 mm^3

Fig.11 Photograph of the L-band SiGe HBT dual-band differential amplifier having frequency-tunable bandpass responses

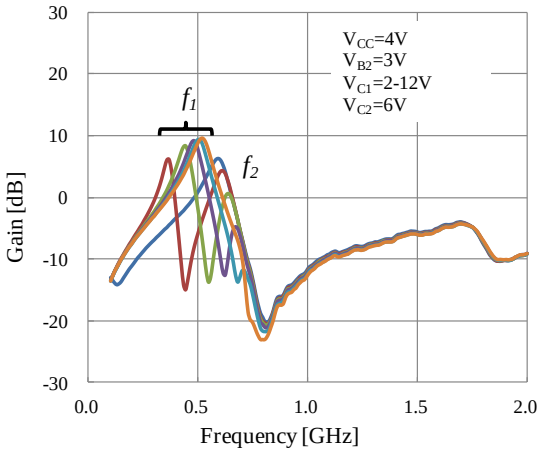

Fig.12 Measured gains of the L-band SiGe HBT dual-band differential amplifier having frequency-tunable bandpass responses for a variable C_1 and a fixed C_2

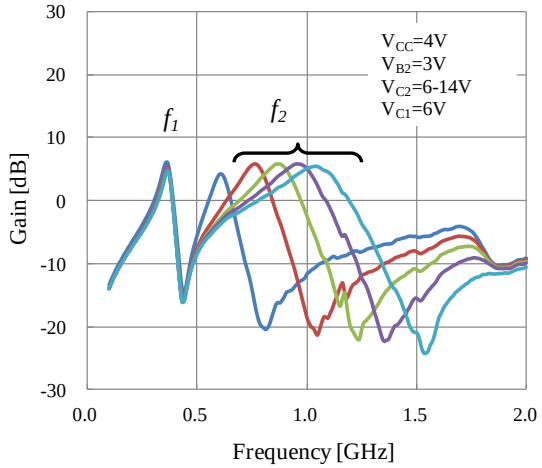

Fig.13 Measured gains of the L-band SiGe HBT dual-band differential amplifier having frequency-tunable bandpass responses for a variable C_2 and a fixed C_1

Measured gains of the L-band SiGe HBT dual-band differential amplifier having frequency-tunable bandpass responses are shown in Fig. 12 for a variable C_1 and a fixed C_2 as well as in Fig. 13 for a variable C_2 and a fixed C_1. Contrary to the dual-bandstop amplifier in Fig. 6, the value of C_2 was chosen as a large value, that is, V_{C2} is small. Therefore, f_1 and f_2 have come closer and finally overlapped. In Fig. 12, the lower-bandstop frequency was varied from 0.37 to 0.5 GHz with an upper-bandstop frequency of 0.61 to 0.63 GHz. Meanwhile, the upper-bandstop frequency can be varied from 0.61 to 1.11 GHz for a lower-bandstop frequency of around 0.36 GHz in Fig. 13. The maximal gain was 9.6 dB. The bias conditions

for V_{CC}, V_{B2}, V_{C1} and V_{C2} are also shown in Figs. 12 and 13. A collector current was around 8mA.

5 Conclusions

Design, fabrication and performance of the L-band SiGe HBT dual-band differential amplifiers with frequency-tunable bandpass or bandstop responses have been presented. The implemented amplifiers have demonstrated excellent frequency-tunable dual-bandpass or dual-bandstop responses with high stability. These results clearly demonstrate that the varactor-loaded dual-bandpass or dual-bandstop differential amplifier presented in this paper would be useful for the next generation adaptive and/or reconfigurable wireless transceivers using the active phased array antennas with beam-forming networks.

References

[1] A. R. Rofougaran, M. Rofougaran and A. Behzad, Radios for Next-Generation Wireless Networks, *IEEE Microwave Magazine*, **6** (2005), 38-43.
http://dx.doi.org/10.1109/mmw.2005.1417993

[2] J. F. Luy, T. Muceller, T. Mack and A. Terzis, Configurable RF Receiver Architectures, *IEEE Microwave Magazine*, **5** (2004), 75-82.
http://dx.doi.org/10.1109/mmw.2004.1284946

[3] G. R. Aiello and G. D. Rogerson, Ultra-Wideband Wireless Systems, *IEEE Microwave Magazine*, **4** (2003), 36-47.
http://dx.doi.org/10.1109/mmw.2003.1201597

[4] A. Raghavan, E. Gebara, M. Tentzeris, J. Laskar, An Active Interference Canceller for Multistandard Collocated Radio, *IEEE MTT-S International Microwave Symposium Digest*, (2005), 723-726.
http://dx.doi.org/10.1109/mwsym.2005.1516712

[5] H. Hashemi and A. Hajimiri, Concurrent Multiband Low-Noise Amplifiers -Theory, Design, and Applications, *IEEE Trans. MTT*, **50** (2002), no. 1, 288-301.
http://dx.doi.org/10.1109/22.981282

[6] Y. T. Lin and S. S. Lu, A 2.4/3.5/4.9/5.2/5.7-GHz concurrent multiband low noise amplifier using InGaP/GaAs HBT Technology, *IEEE Microwave and Wireless Components Letters*, **14** (2004), no. 10, 463-465.
http://dx.doi.org/10.1109/lmwc.2004.834548

[7] H. Nakajima and M. Muraguchi, Dual-Frequency Matching Technique and Its Application to an Octave-Band (30-60 GHz) MMIC Amplifier, *IEICE Transaction*

on Electronics, **E80-C** (1997), no. 12, 1614-1621.

[8] S. O. Yun and H. J. Yoo, Multi-Standard CMOS Power Amplifier with Reconfigurable Matching Networks, *IEICE Trans. Fundamentals*, **E85-A/B/C/D** (2002), no. 1, 1-7.

[9] W. Chen, S. Chang, G. Huang, Y. Jean, T. Yeh, A Ku-Band Interference-Rejection CMOS Low-Noise Amplifier Using Current-Reused Stacked Common-Gate Topology, *IEEE Microwave and Wireless Components Letters*, **17** (2007), no. 10, 718-720. http://dx.doi.org/10.1109/lmwc.2007.905631

[10] T. Nguyen, N. Oh, C. Cha, Y. Oh, G. Ihm, S. Lee, Image-Rejection CMOS Low-Noise Amplifier Design Optimization Techniques, *IEEE Transaction on Microwave Theory and Techniques*, **53** (2005), no. 2, 538-547. http://dx.doi.org/10.1109/tmtt.2004.840744

[11] D. Jachowski, Compact, Frequency-Agile, Absorptive Bandstop Filters, *IEEE MTT-S International Microwave Symposium Digest*, (2005), 513-516. http://dx.doi.org/10.1109/mwsym.2005.1516645

[12] Y. Itoh, L-Band SiGe HBT Differential Amplifiers with Multiple Bandpass or Bandstop Performance Using Stacked Parallel-Resonant Circuits, *Contemporary Engineering Sciences*, **1** (2008), no. 3, 127-138.

[13] M. Shirata, T. Shinohara, M. Sato and Y. Itoh, An L-Band SiGe HBT Differential Amplifier with Frequency and Rejection-Level Tunable, Multiple Stopband, *International Journal of Microwave and Wireless Technologies*, **1** (2009), no. 4, 285-292. http://dx.doi.org/10.1017/s1759078709990390

[14] Y. Itoh, T. Shinohara, M. Shirata, K. Sakamoto, Eightfold-Band Differential SiGe HBT Amplifier Using Stacked LC-Tank Circuits, *Asia-Pacific Microwave Conference*, (2008), 1-4. http://dx.doi.org/10.1109/apmc.2008.4957910

[15] K. Sakamoto and Y. Itoh, L-Band SiGe HBT Frequency-Tunable Dual-Bandpass or Dual-Bandstop Differential Amplifiers Using Varactor-Loaded Series and Parallel LC Resonators, *IEICE Trans. Electron.*, **E95-C** (2012), no. 12, 1839-1845. http://dx.doi.org/10.1587/transele.e95.c.1839

Received: April 29, 2016; Published: July 3, 2016